Supporting Material for: Superionicity and Polymorphism in Calcium Fluoride at High Pressure

Claudio Cazorla*

School of Materials Science and Engineering,

University of New South Wales, Sydney NSW 2052, Australia

Daniel Errandonea

Departamento de Física Aplicada (ICMUV),

Universitat de Valencia, 46100 Burjassot, Spain

Abstract

In this supplemental document we explain the details of our *ab initio* density functional theory calculations and crystal structure searches performed in CaF_2 under pressure. Also we report the computed P-dependence of the formation energy of Frenkel pair defects in the cubic fluorite phase, a sketch of the atomic displacements associated to the zone-boundary X_2 phonon mode, and the vibrational phonon spectra and structural data of the predicted high-T monoclinic $P2_1/c$ phase. Calculated enthalpy energies in compressed SrF_2 and BaF_2 are also presented.

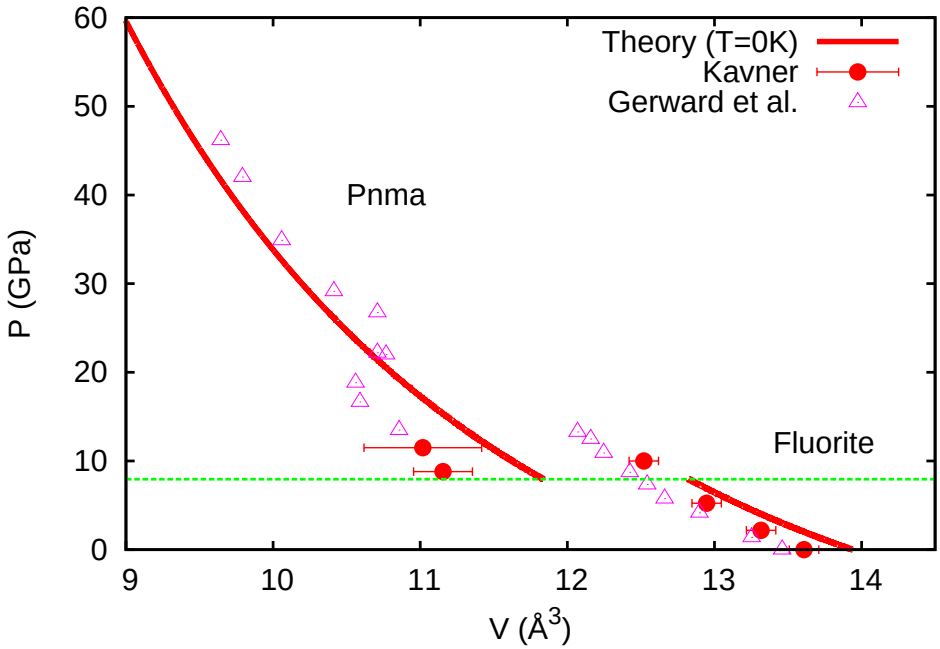

FIG. 1: [Supplemental](Color online) Calculated (solid red line) and measured equation of state of CaF_2 at low temperatures. Experimental data are from works [1,2].

I. ZERO-TEMPERATURE DFT CALCULATIONS

Total energy calculations were carried out in CaF_2 under pressure in the cubic fluorite and orthorhombic cotunnite phases, employing the methods and parameters described in the main text of the present Letter. As it may be appreciated in the supplemental Fig. 1, the agreement between our calculated equation of state and experimental data from Refs. [1,2] is remarkably good. Also we obtain good agreement with measurements done by Dorfman et al. [20] on the volume reduction and bulk modulus variation occurring during the fluorite to contunnite phase transition (i.e., 8 % and 0.2 % , respectively)

In order to calculate the vibrational phonon frequencies of CaF_2, we employed the direct approach [3,4]. In this method, the force-constant matrix is directly calculated in real-space by considering the proportionality between the atomic displacements and forces when the former are sufficiently small. Large supercells must then be constructed in order to guarantee that the elements of the force-constant matrix have all fallen off to negligible values at their boundaries, a condition that follows from the use of periodic boundary conditions. In the present work, we employed simulation boxes larger than 216 atoms and dense **k**-point grids

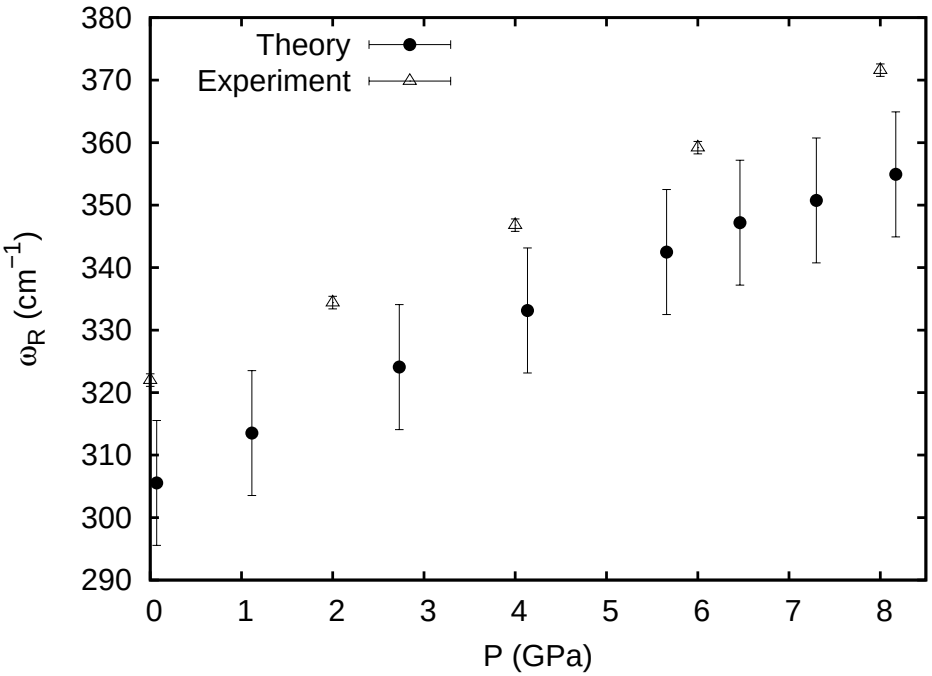

FIG. 2: [Supplemental] Measured and calculated Raman frequencies in α-CaF_2 at low temperatures and expressed as a function of pressure.

in the calculation of the atomic forces with VASP. Computation of the nonlocal parts of the pseudopotential contributions was performed in reciprocal, rather than real, space. Once the force-constant matrix is thus obtained, we can Fourier transform it to obtain the phonon spectrum at any $\mathbf{q}$ point. This step was done with the PHON code due to Alfè [5]. In using this code, we exploited the translational invariance of the system to impose the three acoustic branches to be exactly zero at the $\mathbf{q}$ point, and used central differences in the atomic forces (i.e., we considered positive and negative atomic displacements).

We must note, however, that convergence of the force-constant matrix elements with respect to the size of the supercell in ionic materials may be slow due to the appearance of charge dipoles and macroscopic electric fields in the limit of zero wave vector. Fortunately, long-range dipole-dipole interactions can be modeled at the harmonic level from knowledge of the atomic Born effective charge tensors and the dielectric tensor of the material [6,7]. Taking advantage of this result, Wang *et al.* proposed a mixed-space approach in which accurate force constants are calculated with the direct approach in real space and long-range dipole-dipole interactions with linear response theory in reciprocal space [8,9]. In the present work, we used Wang *et al.* mixed-space approach to calculate the vibrational phonon

frequencies of CaF_2 at different volumes.

In the supplemental Fig. 2, the Raman frequencies that we have measured ($T = 300$ K) and calculated ($T = 0$ K) in α-CaF_2 under compression are represented. The agreement between our measurements and calculations is good (i.e., within the 5 % of difference), especially in what concerns the variation of the Raman frequency with pressure which is found to be almost constant and equal to 6.0 cm^{-1}/GPa in the experiments and 6.2 cm^{-1}/GPa in the simulations. Our measurements in the supplemental Fig. 2 accomodate systematically above our zero-temperature calculations; the likely explanation for such modest differences are thermal excitations. Both our experimental and theoretical results also are in good agreement with previous experiments [10].

II. ONE-PHASE AND TWO-PHASE COEXISTENCE *AB INITIO* MOLECULAR DYNAMICS SIMULATIONS

Our *ab initio* molecular dynamics (AIMD) calculations were of two types: one-phase (i.e., solid and superionic phases) and two-phase coexistence (i.e., liquid and superionic phases coexisting in thermodynamic equilibrium) simulations. One-phase simulations were performed in the canonical (N, V, T) ensemble while two-phase coexistence simulations in the microcanonical (N, V, E) ensemble. In the (N, V, T) simulations the temperature was kept fluctuating around a set-point value by using Nose-Hoover thermostats. Large simulation boxes containing 192 and 648 atoms were used in our one-phase and two-phase coexistence simulations, respectively. Periodic boundary conditions were applied along the three Cartesian directions in all the calculations. Newton's equations of motion were integrated using the customary Verlet's algorithm and a time-step length of 10^{-3} ps. Γ-point sampling for integration within the first Brillouin zone was employed in all our AIMD simulations.

Comprehensive one-phase (N, V, T) molecular dynamics simulations were carried out in order to compute the $\alpha - \beta$ and $\delta - \epsilon$ phase boundaries in CaF_2 as a function of pressure. Calculations comprised large simulation boxes and long simulation times of up to ~ 30 ps. We systematically carried out simulations at temperature intervals of 250 K, from 1000 up to 3500 K, at each considered volume.

Following previous works [11–16], we performed comprehensive (N, V, E) two-phase coexistence MD simulations in order to determine the melting curve of CaF_2 at low and high

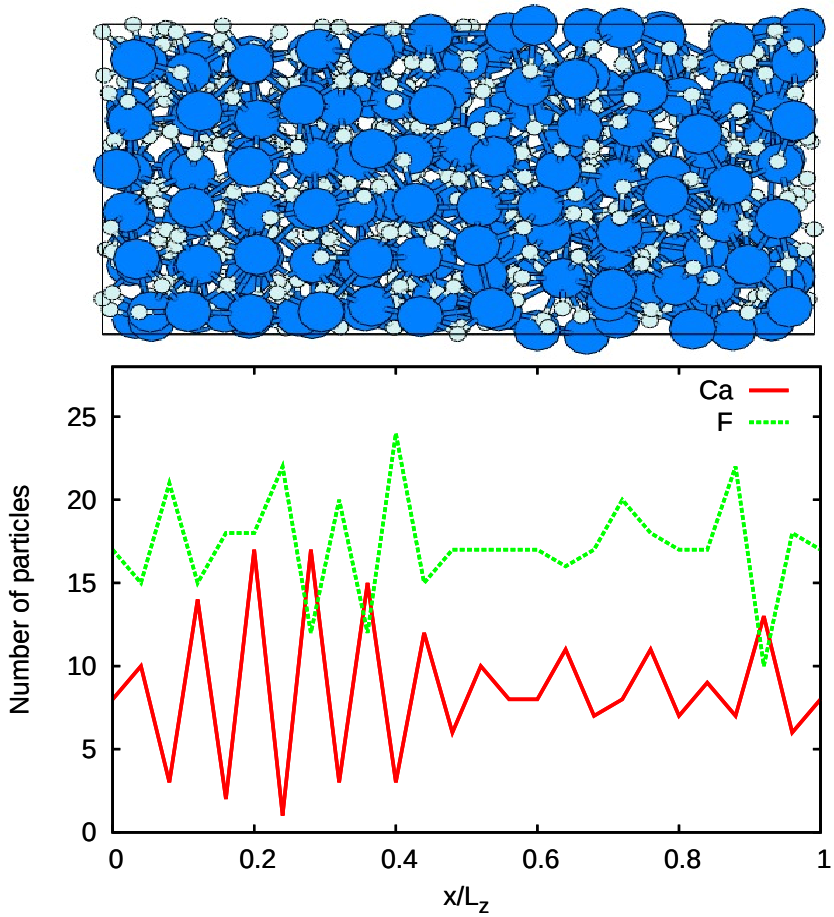

FIG. 3: [Supplemental](Color online) Determination of melting temperatures based on two-phase coexistence *ab initio* molecular dynamics simulations. *Top*: Atomic positions projected over the $x-y$ plane of the simulation box. Calcium and fluorine ions are represented with large (dark blue) and small (bright blue) spheres, respectively. *Bottom*: Number of particles histogram represented as a function of position along the direction parallel to the initial superionic-liquid boundary.

pressures. Starting with a supercell containing the perfect crystal structure (i.e. either cubic fluorite or orthorhombic $Pnma$), we thermalize it at a temperature slightly below the expected melting temperature for about 4 ps. The system remains in a superionic state. The simulation is then halted and the positions of the atoms in one half of the supercell are held fixed while the other half is heated up to a very high temperature (typically five times the expected melting temperature) for about 4 ps, so that it melts completely. With the fixed atoms still fixed, the molten part is rethermalized to the expected melting temperature (for about 2 ps). Finally, the fixed atoms are released, thermal velocities are assigned, and the whole system is allowed to evolve freely at constant (N, V, E) for a long time (normally more

than 20 ps), so that the solid and liquid come into equilibrium. The system is monitored by calculating the average number of particles in slices of the cell taken parallel to the boundary between the solid and liquid. With this protocol, there is a certain amount of trial and error to find the overall volume which yields the coexisting solid and liquid system. An example of a successful coexistence run is shown in the supplemental Fig. 3.

III. FORMATION ENERGY OF FRENKEL PAIR DEFECTS UNDER PRESSURE AND THE X_2 PHONON MODE

We calculated the formation energy of Frenkel pair defects (FPD) in cubic CaF_2 at different pressures. We used a simulation box containing 96 atoms and a $2\times2\times2$ Monkhorst-Pack **k**-point grid for integrations within the first Brillouin zone. We found that the series of calculated energies (see the supplemental Fig. 4) could be very well fitted to the power law function

$$E_{FPD}(P) = E_0 + a \cdot P^b \ , \tag{1}$$

where the optimal values of the parameters are $E_0 = 2.07$ eV, $a = 0.054$ eV and $b = 0.851$. It is noted that the formation energy of FPD increases monotonically and appreciably with compression.

In the supplemental Fig. 5, we present a sketch of the atomic displacements associated to the zone-boundary X-phonon mode calculated in α-CaF_2, which exhibits softening under increasing P. The atomic pattern associated to this vibrational eigenmode implies displacements of rows of F ions in opposed directions along the [-1, 1, 1] axis (in Cartesian coordinates). This sketch is consistent with the generally accepted view of superionicity in α-CaF_2, where the F anions present disorder within the perfect lattice formed by the Ca cations. We note that occurrence of these collective vibrational excitations in the crystal do not exclude the formation of Frenkel pair defects in the same.

IV. CRYSTAL STRUCTURE SEARCHES

Our crystal structure searches performed in compressed CaF_2 relied on two different strategies, namely (i) comprehensive atomic relaxations of configurations generated in constrained low-T AIMD runs, and (ii) enthalpy calculation of phases that have been recently

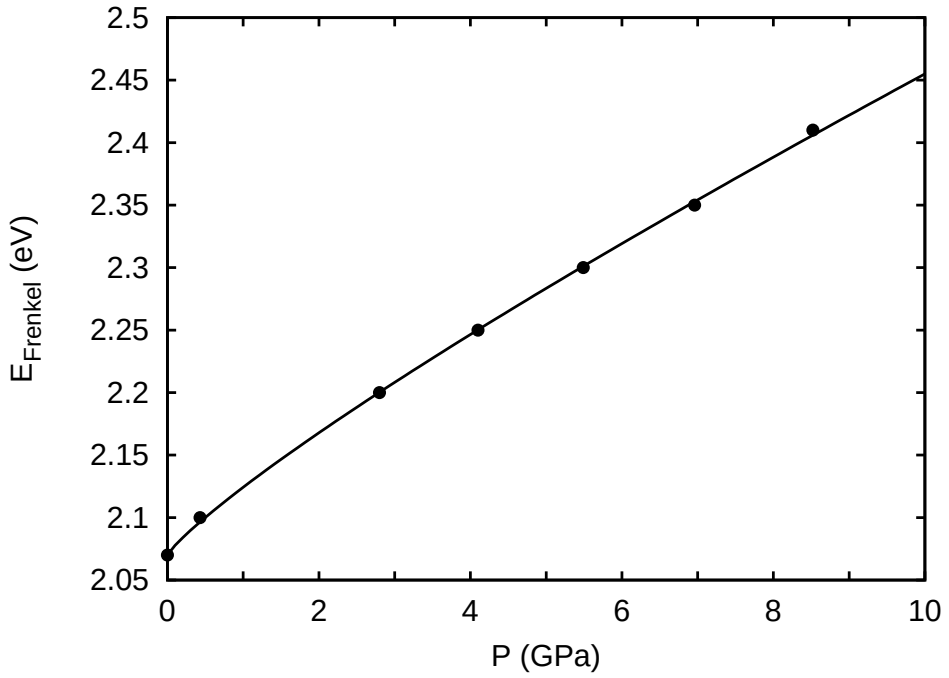

FIG. 4: [Supplemental] Calculated formation energy of Frenkel pair defects in α-CaF_2 under pressure. The solid line represents a numerical fit to the series of computed points (see text).

observed and predicted in isomorphic AB_2 compounds under pressure.

In our restricted low-T AIMD runs, we used a small simulation cell containing 24 atoms in the orthorhombic $Pnma$ phase and set the temperature to ambient conditions. Consistently to the observed $\gamma \rightarrow \delta$ transition, we constrained the Ca^{2+} cations not to move during the dynamical simulations. The total duration of these AIMD runs was $\sim$ 20 ps. Once these simulations were finished, we randomly selected 100 configurations out of $10,000$ and performed atomic and crystal cell relaxations in them. During the geometry optimizations all cations and anions were allowed to move. Subsequently, we identified the crystal symmetry of the final equilibrium structures with the ISOTROPY package [17]. Following this strategy, we obtained the five candidate high-T crystal phases that we mention in the main text of the present Letter (i.e., orthorhombic $P2_12_12_1$ and $Pmn2_1$, and monoclinic Pc, $P2_1$ and $P2_1/c$).

We also computed the energy of the post-cotunnite $P112_1/a$ and $P2_1/n$ phases in CaF_2 under pressure. These phases have been recently observed and predicted in bulk $AuIn_2$ and $AuGa_2$ respectively [18,19], which are isomorphic materials to CaF_2. By following this strategy, however, we did not find any promising high-T candidate crystal phase since their

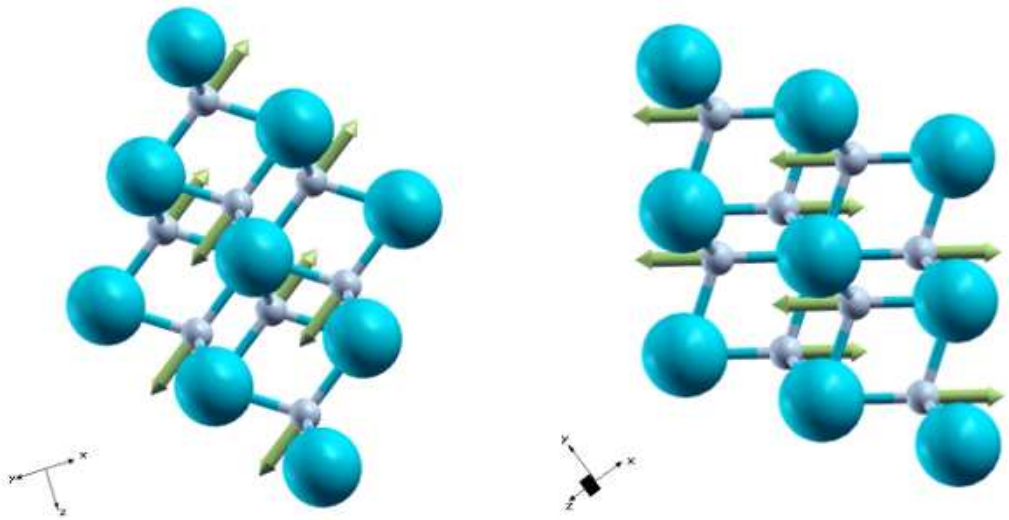

FIG. 5: [Supplemental] Sketch of the zone-boundary X_2-phonon mode calculated in α-CaF_2, which softens under pressure. The arrows indicate the eigenmode atomic displacements, and the small and large spheres F and Ca ions, respectively. Two different views are presented.

corresponding enthalpies were too large in comparison to those of the crystal structures obtained with strategy (i).

V. STRUCTURAL DATA, PHONONS AND ENTHALPY OF THE PREDICTED HIGH-T MONOCLINIC $P2_1/c$ PHASE

A sketch of the new high-T monoclinic $P2_1/c$ phase predicted in CaF_2 at high-P is shown in the supplemental Fig. 6. This structure has a similar cation coordiantion polyhedra to that of the orthorhombic $Pnma$ phase. On it each calcium is coordinated to 9 fluorine atoms that form an elongated tricapped trigonal prism. Structural data of this monoclinic phase obtained at different pressure conditions are enclosed in Table I.

We computed the phonon spectrum of this high-T monoclinic phase at different pressures employing the methodology explained in this supplemental document (see Sec. I), and found that it was vibrationally and mechanically stable (see the supplemental Fig. 7).

The results of our enthalpy calculations in SrF_2 and BaF_2 compounds are enclosed in

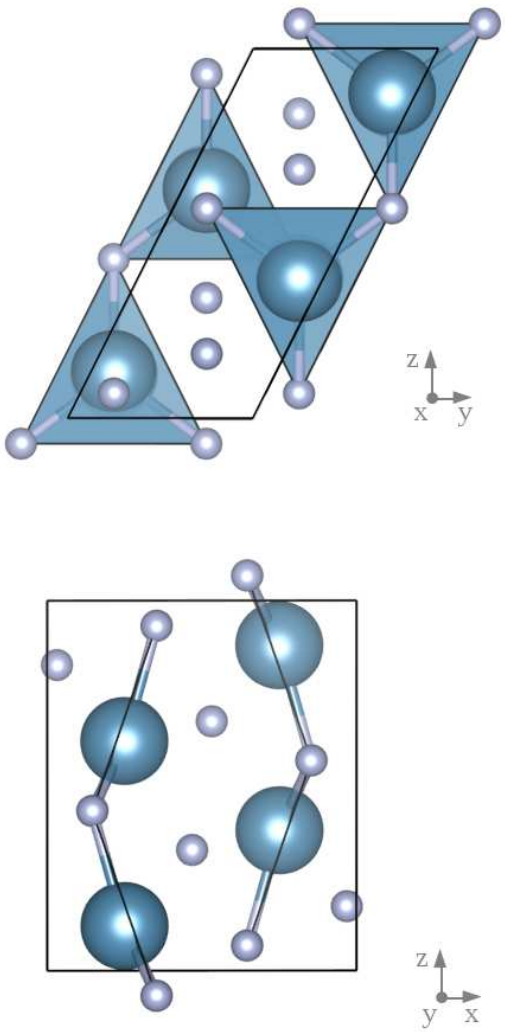

FIG. 6: [Supplemental](Color online) Sketch of the predicted high-T monoclinic $P2_1/c$ phase. Large (Blue) and small (grey) spheres represent calcium and fluorine atoms, respectively.

the supplemental Fig. 8. In particular, we computed the enthalpy energy of the cubic fluorite, orthorhombic $Pnma$, hexagonal $P6_3/mmc$, and monoclinic $P2_1/c$ phases in the corresponding pressure regimes of interest. As we found in CaF_2, the monoclinic $P2_1/c$ phase turns out to be energetically very competitive with respect to the orthorhombic $Pnma$ phase, and actually under some conditions the enthalpy difference between the two phases is zero within our numerical accuracy (i.e., 3 meV/f.u.).

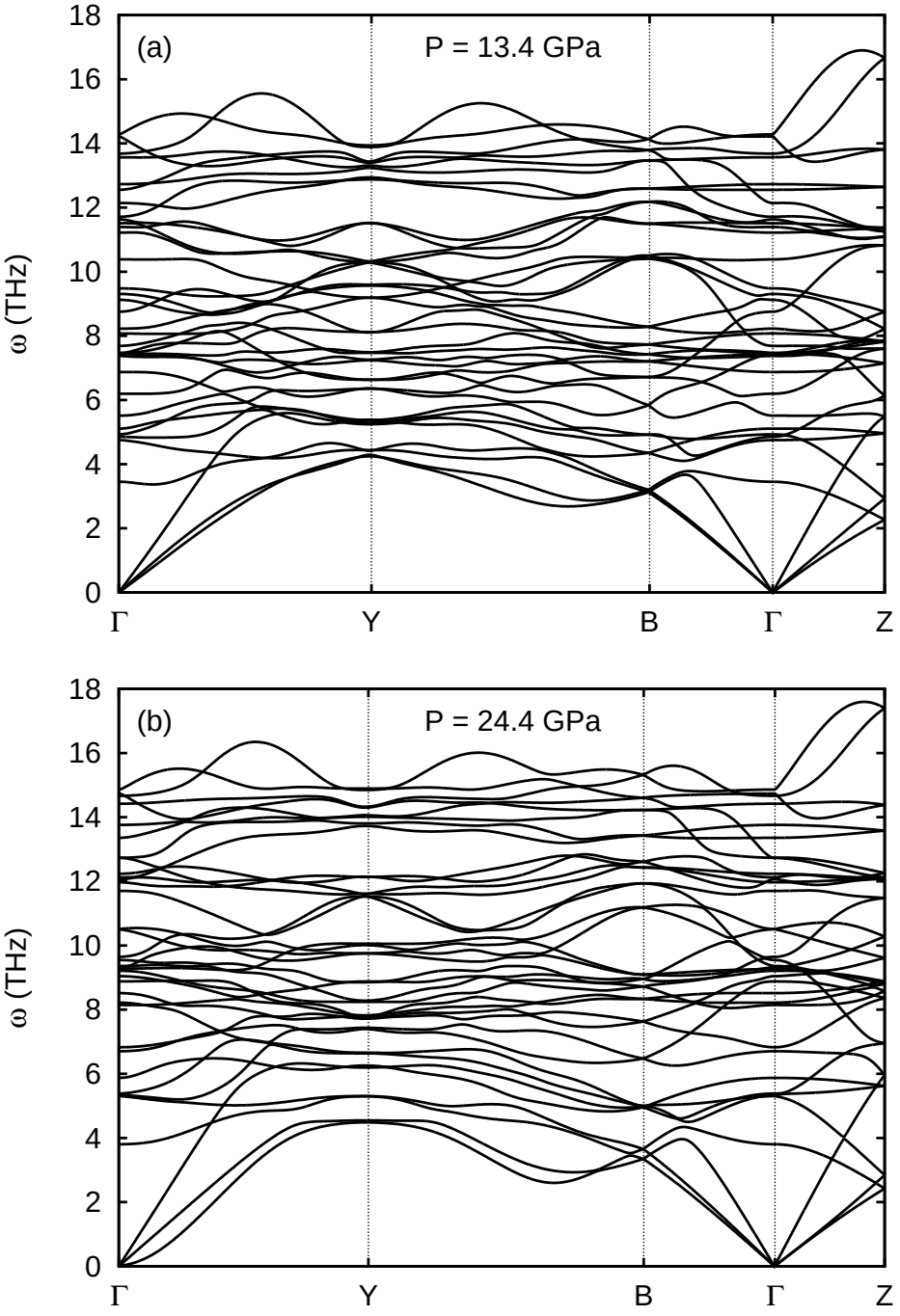

FIG. 7: [Supplemental] Calculated phonon spectrum of the predicted high-T monoclinic $P2_1/c$ phase at different pressures.

$P2_1/c$	$a = 3.347$ Å	$b = 6.032$ Å	$c = 7.477$ Å
(P = 13.4 GPa)	$\alpha = 90$ °	$\beta = 116.6$ °	$\gamma = 90$ °

Atom	Wyc.	x	y	z
Ca	4e	0.37156	0.75481	0.12145
F	4e	0.31867	0.14034	0.06867
F	4e	0.08291	0.53005	0.83343

$P2_1/c$	$a = 3.353$ Å	$b = 5.620$ Å	$c = 7.477$ Å
(P = 24.4 GPa)	$\alpha = 90$ °	$\beta = 116.6$ °	$\gamma = 90$ °

Atom	Wyc.	x	y	z
Ca	4e	0.36963	0.75135	0.11987
F	4e	0.31873	0.14546	0.06872
F	4e	0.07811	0.52958	0.82824

TABLE I: [Supplemental] Structural data of the predicted high-T monoclinic $P2_1/c$ phase calculated at different pressures. Wyckoff positions were generated with the ISOTROPY package[17].

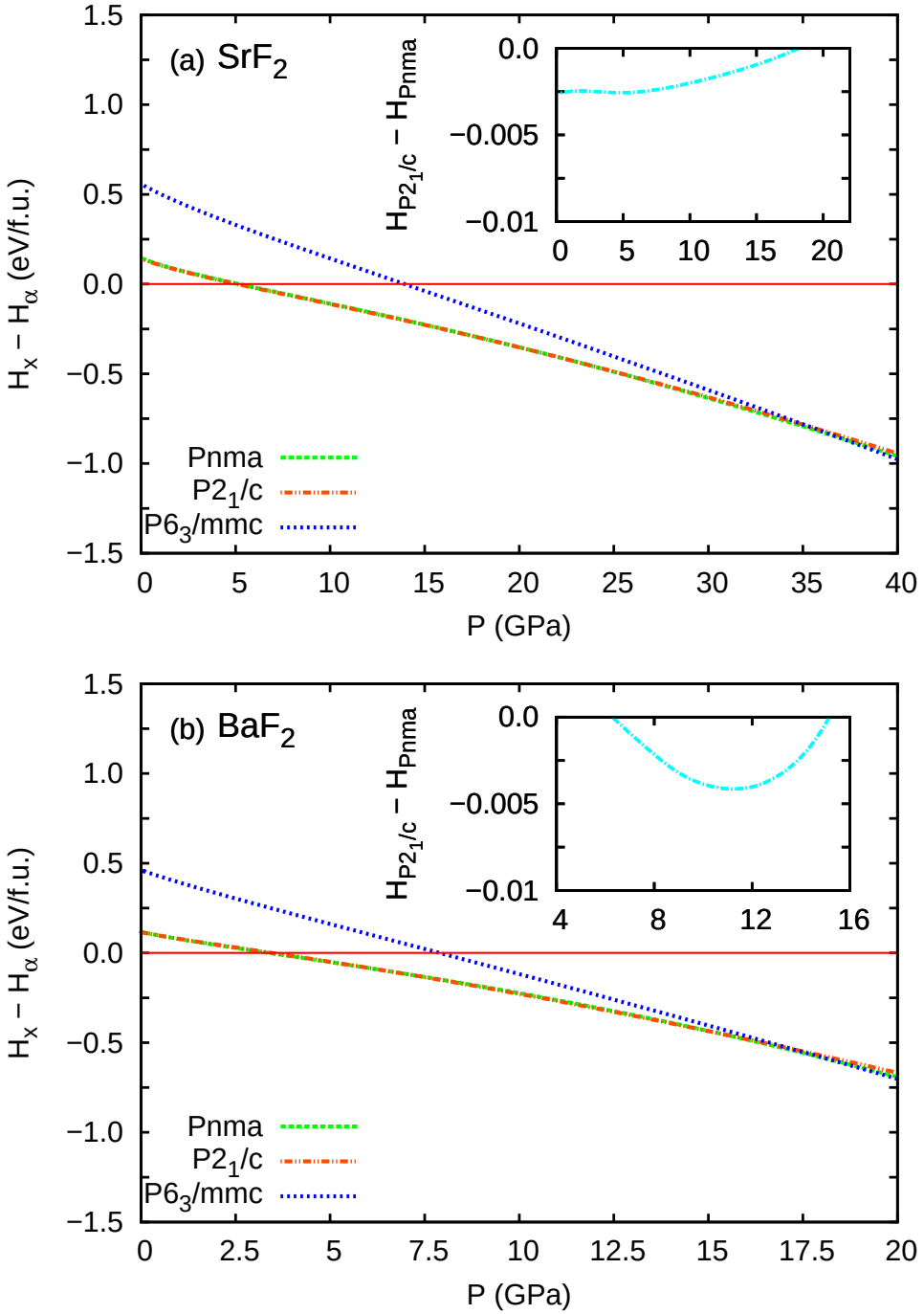

FIG. 8: [Supplemental] Calculated enthalpy of several crystal structures referred to that of the cubic α phase and expressed as a function of pressure in SrF_2 and BaF_2. *Inset*: Detail of the enthalpy difference between the $P2_1/c$ and $Pnma$ phases.

* Electronic address: ccazorla@icmab.es; Corresponding Author

[1] A. Kavner, Phys. Rev. B **77**, 224102 (2008).

[2] L. Gerward, J. S. Olsen, S. Steenstrup, M. Malinowski, S. Asbrink, and A. Waskowska, J. Appl. Crystallogr. **25**, 578 (1992).

[3] G. Kresse, J. Fürthmuller, and J. Hafner, Europhys. Letter. **32**, 729 (1995).

[4] D. Alfè, G. D. Price, and M. J. Gillan, Phys. Rev. B **64**, 045123 (2001).

[5] D. Alfè, Comput. Phys. Commun. **180**, 2622 (2009).

[6] X. Gonze and J.-P. Vigneron, Phys. Rev. B **39**, 13120 (1989).

[7] S. Baroni, S. de Gironcoroli, A. del Corso, and P. Giannozzi, Rev. Mod. Phys. **73**, 515 (2001).

[8] Y. Wang, J. J. Wang, W. Y. Wang, Z. G. Mei, S. L. Shang, L. Q. Chen, and Z. K. Liu, J. Phys.: Condens. Matter **22**, 202201 (2010).

[9] C. Cazorla and J. Íñiguez, Phys. Rev. B **88**, 214430 (2013).

[10] S. Speziale and T.S. Duffy, Phys. Chem. Minerals **29**, 465 (2002).

[11] C. Cazorla, M. J. Gillan, S. Taioli, and D. Alfè, J. Chem. Phys. **126**, 194502 (2007).

[12] S. Taioli, C. Cazorla, M. J. Gillan, and D. Alfè, Phys. Rev. B **75**, 214103 (2007).

[13] C. Cazorla, D. Alfè, and M. J. Gillan, J. Chem. Phys. **130**, 174707 (2009).

[14] D. Alfè, C. Cazorla and M. J. Gillan, J. Chem. Phys. **135**, 024102 (2011).

[15] C. Cazorla, D. Alfè, and M. J. Gillan, Phys. Rev. B **85**, 064113 (2012).

[16] D. Alfè, Phys. Rev. B **79**, 060101(R) (2009).

[17] H. T. Stokes, D. M. Hatch, and B. J. Campbell, (2007). *ISOTROPY, stokes.byu.edu/isotropy.html*.

[18] B. K. Godwal, S. Speziale, M. Voltolini, R. Wenk, and R. Jeanloz, Phys. Rev. B **82**, 064112 (2010).

[19] B. K. Godwal, S. Stackhouse, J. Yan, S. Speziale, B. Militzer, and R. Jeanloz, Phys. Rev. B **87**, 100101(R) (2013).

[20] S. M. Dorfman, F. Jiang, Z. Mao, A. Kubo, Y. Meng, V. B. Prakapenka, and T. S. Duffy, Phys. Rev. B **81**, 174121 (2010).